Article

Direct quantification by infrared spectroscopy of drug loading content in polymeric nanoparticles

Guzmán Carissimi [1], Mercedes G. Montalbán[1], Gloria Víllora[1] and Andreas Barth[2,*]

[1] Department of Chemical Engineering, Faculty of Chemistry, University of Murcia, Murcia 30100, Spain; guzmanaugusto.carissimin@um.es (G.C.); mercedes.garcia@um.es (M.G.M.); gvillora@um.es (G.V.)

[2] Department of Biochemistry and Biophysics, Stockholm University, Stockholm SE-106 91, Sweden

* Correspondence: barth@dbb.su.se

Abstract: Nanotechnology has enabled the development of novel therapeutic strategies such as targeted nanodrug delivery systems, control and stimulus-responsive release mechanisms, and the production of theranostic agents. As a prerequisite for the use of nanoparticles as drug delivery systems, the amount of loaded drug must be precisely quantified, a task for which two approaches are currently used. However, both approaches suffer from the inefficiencies of drug extraction and of the solid-liquid separation process, as well as from dilution errors. This work describes a new, reliable, and simple method for direct drug quantification in polymeric nanoparticles using attenuated total reflection Fourier transform infrared spectroscopy, which can be adapted for a wide variety of drug delivery systems. Silk fibroin nanoparticles and naringenin were used as model polymeric nanoparticle carrier and drug, respectively. The specificity, linearity, detection limit, precision and accuracy of the spectroscopic approach were determined in order to validate the method. A good linear relation was observed within 0.00 to 7.89 % of naringenin relative mass with an R^2 of 0.973. The accuracy was determined by the spike and recovery method. Results showed an average 104% recovery. The limit of detection and limit of quantification of the drug loading content were determined to be 0.3 and 1.0 %, respectively. The method's robustness is demonstrated by the notable similarities between the calibrations carried out in two different equipment and institutions.

Keywords: silk fibroin; nanoparticles; drug loading content; quantification; infrared spectroscopy; FTIR spectroscopy, nanotechnology, nanomedicine, drug delivery, controlled release.

1. Introduction

The use of nanoparticles as drug delivery systems is already a reality with more than 50 FDA-approved nanomedicines being used in April-2016, and more to come in the foreseeable future [1]. The use of nanoparticles as delivery systems may provide numerous benefits [2–4], including an enhanced drug delivery to tumor cells [5,6], controlled release and improved biodistribution [7], all of which result in a reduction of drug side effects [8,9]. Among polymeric nanoparticles used as delivery systems, silk fibroin-based nanoparticles (SFN) from the silkworm *Bombyx mori* have shown promising results, partly due to their biodegradability, biocompatibility and non-toxicity [10–16]. Their ability to penetrate biological membranes and their high drug loading capacity means that SFN can greatly improve therapeutic treatments [17,18]. Furthermore, the SFN surface can be functionalized by attaching recognition molecules for targeted delivery such as peptides or other small molecules [19,20].

However, if nanoparticles are to be used as drug delivery systems, the amount of loaded drug must be precisely quantified. Up to date, two approaches are mostly used for this task. They are based on a direct and indirect measurement of the drug loading content (DLC) in the nanoparticle. In the indirect approach [21–25], a fresh loading solution of the drug is prepared and measured before adding the nanoparticles. The suspension is stirred, and at the end of the loading process [13], the particles are separated from the loading solution, typically by centrifugation or filtration, and the remaining drug in the supernatant solution is measured. Finally, the amount of drug in the

 doi:10.20944/preprints202009.0047.v1

nanoparticles is calculated by a mass balance. However, as high drug concentrations are normally used for the loading solution, large dilution factors are needed to keep the analyte signal in the equipment's operating range (usually UV-visible spectrophotometry or high-pressure liquid chromatography), adding uncertainty and thus lowering the accuracy and the precision. Furthermore, this approach cannot be used for independent control of the drug content of the final product because only the producer will have access to the loading solution. Further still, the drug content may change upon storage in which case an analysis of the loading solution will be meaningless.

As for the direct approach [26–29], the drug from the loaded particles is extracted with a suitable solvent, then particles are sedimented and the drug in the supernatant is measured. However, it has been shown that separation methods such as filtration or centrifugation are not always effective for separating nanoparticles from the liquid phase, leading to errors in spectroscopic measurements [30,31]. Even so, extracting the total drug loaded is difficult and hard to verify. Moreover, both methods assume that the drug absorption is in the UV-visible range and that there is no interference with the nanoparticles and their dissociated components that may remain in dispersion after the separation process.

For these reasons, this work develops a reliable and simple method for directly quantifying drugs in nanoparticle dispersions/suspensions which can be adapted for use with other types of nanostructures also. To the best of our knowledge, this is the first time that attenuated total reflection - Fourier transform infrared (ATR-FTIR) spectroscopy has been used for the direct quantification of the drug-load of nanoparticles. FTIR spectroscopy is a well-established technique within the pharmaceutical industry with applications ranging from qualitative to quantitative analysis [32–37]. In the latter, its major advantage over UV-visible spectroscopy is that practically all compounds absorb IR light and can thus be analyzed. In addition, the IR spectrum typically shows a large number of characteristic absorption bands with limited overlap because they are distributed over a wide spectral range.

As a model drug we used SFN loaded with naringenin (NAR), a natural flavonoid [38,39], which has recently demonstrated its good compatibility with silk fibroin [16]. NAR has received increasing attention in medicine due to its free-radical scavenging [40], anti-inflammatory [41], and anticancer properties [42–46]. However, NAR quantification remains a problem, especially when loaded into protein-based nanoparticles, as its absorption maximum at 289 nm overlaps the absorption of aromatic amino acids of proteins. The robustness of the proposed method is demonstrated by consistent results from two different laboratories in a collaboration between the University of Murcia (UMU, Spain) and Stockholm University (SU, Sweden). The two institutions use different equipment, and their respective latitudes are significantly different meaning that the performance of the method can be compared at different temperatures and in different climate conditions.

2. Materials and Methods

2.1. Materials

The silk fibroin (SF) used in this study was extracted from white silk cocoons of the silkworm *Bombyx mori* reared in the sericulture facilities of IMIDA (Murcia, Spain) with a diet based on fresh *Morus alba L.* leaves. The intact pupae were hand-extracted from the silk cocoons between two to seven days after the spinning process to avoid cross-contamination with the worm. To extract the SF, silk cocoons were shredded in a mill up to 1 mm particle size, and later boiled in 0.2 N Na_2CO_3 solution for 120 minutes to remove sericin, waxes and impurities. The remaining water-insoluble SF was rinsed thoroughly with ultrapure water and air-dried under a fume hood until constant weight. NAR was purchased from Sigma-Aldrich (Madrid, Spain) and was used without further purification. Purified water (18.2 MΩ·cm at 25 ºC; from a Millipore Direct-Q1 ultrapure water system, Billerica, MA) was used throughout.

Preprints (www.preprints.org) | NOT PEER-REVIEWED | Posted: 3 September 2020 doi:10.20944/preprints202009.0047.v1

2.2. Preparation of stock nanoparticle dispersion and drug solution

SFN were prepared as described elsewhere [13][16]. The freeze-dried SFN were dispersed in Milli-Q water by ultrasonication probe to a final concentration of 20 mg/mL. A stock NAR solution was prepared in ethanol by stirring vigorously until complete dissolution at a final concentration of 15 mg/mL. Throughout this work, all the solutions containing NAR were always kept protected from light.

2.3. Calibration samples for NAR in SFN

To calibrate of the ATR-FTIR method, six samples were prepared with a NAR relative mass (*NAR%*) of 0.00, 1.06, 2.10, 4.11, 6.04, and 7.89 %, calculated as described in equation 1, where m_{NAR} and m_{SFN} are the masses of NAR and SFN in the NAR/SFN dispersion, respectively.

$$NAR\% = \frac{m_{NAR}}{m_{NAR} + m_{SFN}} \times 100, \quad (1)$$

Samples were prepared by adding a fixed volume of SFN stock dispersion, followed by a variable volume of NAR stock solution and, finally, a variable volume of pure ethanol so that the total volume was 100 µL. The pure ethanol is added to maintain a constant proportion of 30 % ethanol, thus ensuring that SFN remained totally dispersed and the NAR totally dissolved. The SFN mass was kept constant in all the samples and only the NAR mass was increased between samples. These calibration samples were used to measure the NAR infrared absorption spectrum in the presence of SFN, which contained contributions from free and loaded NAR. The samples were prepared freshly every day and measured in triplicate at SU and UMU giving a total of six calibration lines, all of which were obtained on different days.

2.4. NAR-loaded SFN samples

To test the drug detection and quantification capabilities of ATR-FTIR spectroscopy, three samples of SFN were loaded with NAR by SFN incubation in drug solutions with NAR concentrations of 0.30, 1.2 and 4.5 mg/mL for 24 h. Samples were named SFN_{NAR}-0.3 mg/mL, SFN_{NAR}-1.2 mg/mL and SFN_{NAR}-4.5 mg/mL, according to the concentration of the drug in the loading solution and were prepared in triplicate on different days. The final SFN concentration in each sample was 14 mg/mL and the final volume of the loading sample 100 µL. As for the calibration samples, the loading drug solutions contained 30 % ethanol, thus ensuring that SFN remained totally dispersed and the NAR totally dissolved. Loading SFN/NAR dispersions were sonicated before starting the incubation period to ensure homogeneity. After the incubation time, the nanoparticles were centrifuged for 20 minutes at 12.100 x g, after which the supernatant with the unloaded/unbounded drug was removed. Subsequently, the nanoparticles were washed with 30% EtOH to remove the unbound drug. Finally, drug-loaded nanoparticles were re-dispersed in milli-Q water by ultrasonication before quantification of drug loading.

The drug loading content (*DLC*) and entrapment efficiency (*EE*) of the SFN_{NAR} were calculated according to the following expressions:

$$DLC\ (\%) = \frac{weight of NAR \text{ of in } the\ nanoparticle}{weight\ of\ SFN_{NAR}} \times 100, \quad (2)$$

$$EE\ (\%) = \frac{weight of NAR \text{ of in } the\ nanoparticle}{\text{weight of NAR in loading solution}} \times 100, \quad (3)$$

 doi:10.20944/preprints202009.0047.v1

In equation 2, the *weight of* SFN_{NAR} is the sum of the masses of NAR and SFN in the loaded nanoparticles, making it analogous to equation 1. Thus, *DLC* can be directly read out from our calibration line.

2.5. Spectra Acquisition and Data Pretreatment

The infrared absorption spectra measured at the Stockholm University were recorded on a Vertex 70 Fourier-transform infrared spectrometer (Bruker Optics, Ettlingen, Germany) equipped with a liquid nitrogen-cooled Mercury-Cadmium- Telluride detector and a 1-reflection, 45° angle of incidence diamond ATR accessory (Platinum, Bruker Optics, Ettlingen, Germany). The equipment was continuously purged with CO_2-reduced, dry air. Each measured spectrum was averaged from 300 scans at a data collection rate of 9.38 scans per second.

The infrared absorption spectra measured at the University of Murcia (UMU) were recorded on an iS5-Nicolet Fourier-transform infrared spectrometer (Thermo Fischer Scientific, Waltham, MA, USA) equipped with a Deuterated Triglycine Sulfate detector and a 1-reflection, 45° angle of incidence diamond ATR accessory (iD7 ATR module, Thermo Fischer Scientific, Waltham, MA, USA). Each measured spectrum was the average of 32 scans at a data collection rate of 0.47 scans per second.

In both cases, interferograms were recorded at a resolution of 2 cm^{-1} with a zero-filling factor of 2, and Fourier-transformed using the Blackman-Harris 3-term apodization function. A background spectrum without a sample with the same number of scans was collected before each measurement. The spectra of the samples were acquired in the form of dry films by placing 2.5 µL of the nanoparticle dispersion on top of the ATR-crystal and drying it under a gentle stream of nitrogen before measuring as described above. The film thickness may have dramatic effects on the resultant ATR spectrum [47,48]: to obtain reproducible results, the thickness of the dry film must be greater than the penetration depth of the evanescent wave into the sample. To ensure this, we placed a piece of plastic tape on top of the dry film sample, applied pressure with the ATR press, and then took the measurement. The absence of tape signals in the spectrum guaranteed that the penetration depth of the evanescent wave was smaller than the thickness of the dry film and hence that the amount of sample placed on the ATR crystal was sufficient. This procedure was performed only once, then the volume and concentration were kept constant for the rest of the experimentation.

As a pretreatment for drug quantification, each spectrum was truncated to the region between 1350 and 900 cm^{-1}, then a baseline was subtracted by tracing straight lines between the minima of the SFN spectrum at 1350, 1316, 1185, 1134 and 900 cm^{-1}. Finally, the absorbance scale was normalized to 1 for the amide III band of silk fibroin (1229 cm^{-1}). The 1085 cm^{-1} band of NAR was chosen to quantify NAR content in SFN because of its high absorption coefficient and its insensitivity to NAR incorporation into SFN (see Results and discussion). The calibration samples were used to establish a correlation between the amount of NAR and the absorbance at 1085 cm^{-1} as described in Results and discussion.

3. Results and Discussion

3.1. Specificity of ATR-FTIR spectroscopy for identifying drugs in SFN

The specificity of ATR-FTIR spectroscopy was tested by performing a spectral coincidence match where the spectrum of SFN_{NAR}-0.3 was compared with the pure NAR spectrum. Before comparing the two spectra, a SFN spectrum was subtracted from the SFN_{NAR}-0.3 spectrum. As a consistent subtraction of both the amide I and amide II band of SFN was not possible, our compromise criterion for spectral subtraction, was to obtain a positive and a negative band at the positions of the amide I and II bands, respectively, while trying to maximize signals from NAR. The OMNIC software V9 (Thermo Fischer Scientific) was used to compare the resulting spectrum and the NAR spectrum both of which can be seen in Figure 1. The region from 1700 to 1450 cm^{-1} was distorted by the subtraction of the SFN spectrum due to the presence of the intense amide I and II bands and was excluded from the spectral matching. Only the region from 1400 to 1000 cm^{-1} highlighted by the gray area in the

Preprints (www.preprints.org) | NOT PEER-REVIEWED | Posted: 3 September 2020 doi:10.20944/preprints202009.0047.v1

figure was used for the spectral match. The OMNIC software found a coincidence match of 86%. This result demonstrates that the drug in the nanoparticles could be identified, even when the drug concentration is low.

The result suggests that this approach could also be used with other proteins as drug carriers, because the absorption of the proteins is relatively weak below 1400 cm^{-1}, where the IR spectrum is highly characteristic of the structure of the molecules. Drugs with an appreciable absorption in this fingerprint region of the IR spectrum can, therefore, be identified.

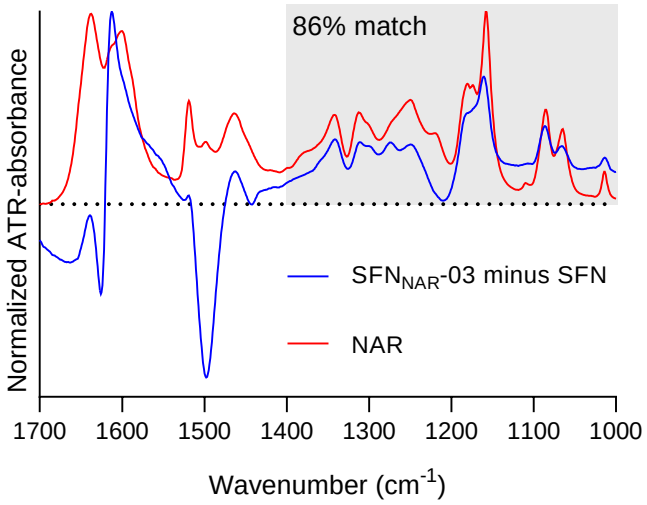

Figure 1. Specificity of ATR-FTIR spectroscopy for identifying drugs in SFN. In blue, the resulting spectrum after subtraction of the SFN spectrum from the SFNNAR-0.3 spectrum. In red, the spectrum of NAR measured from a dried film. The gray rectangle shows the area used for matching.

3.2. *Identification of the best marker band for NAR in SFN$_{NAR}$ samples*

The first step in the quantification process was to identify a strong signal from NAR in the IR spectrum, with low interference from the silk fibroin matrix, to be used to generate a calibration curve. In Figure 2a, the spectra of SFN and NAR are presented from 1750 to 900 cm^{-1}. The SFN spectrum presents the expected amide I, II and III bands at 1620, 1514 and 1229 cm^{-1}, respectively, for silk fibroin protein [49–51].

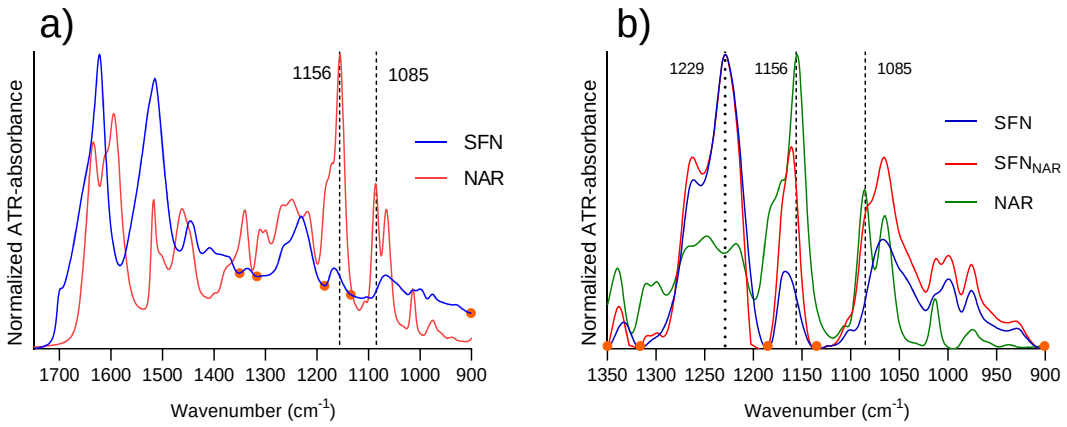

Preprints (www.preprints.org) | NOT PEER-REVIEWED | Posted: 3 September 2020 doi:10.20944/preprints202009.0047.v1

Figure 2. a) Original infrared ATR-absorption spectra of SFN and NAR. b) Base-line corrected infrared ATR-absorption spectra of SFN, NAR and SFN_{NAR}-1.2. The SFN and the SFN_{NAR} spectra are normalized to an absorbance of 1 at the maximum of the amide III band at 1229 cm^{-1}. The NAR spectrum is normalized to an absorbance of 1 at 1156 cm^{-1}. All samples were measured as a dry film obtained from a 30% EtOH solution. Orange dots indicate the baseline points.

The NAR spectrum presents strong absorption bands positioned at 1633, 1609, 1594, 1169, 1156, 1085 and 1065 cm^{-1}. The first three bands arise from vibrations comprising different combinations of C=O stretching, ring C-C stretching and OH bending vibrations [52,53]. The reader can refer to figure 3 for the structure of NAR. These three bands overlap with the strong amide I band of SFN, making NAR detection from these signals rather challenging – therefore, they were not taken into account.

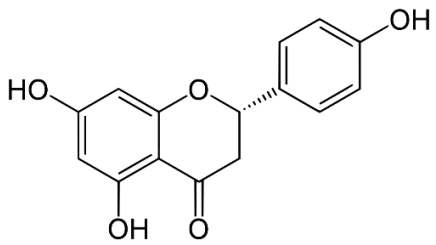

Figure 3. Structure of NAR.

Bands at 1169 and 1156 cm^{-1} arise from a combination of OH and CH_2 bending vibrations [53]. Neither these bands were considered for quantification, as hydroxyls may interact with the protein matrix from SFN, which will cause band shifts upon binding of NAR to SFN. Indeed, it can be seen in Figure 2b that the 1156 cm^{-1} absorption band of NAR is up-shifted by 6 cm^{-1} in the spectrum of NAR-loaded SFN (SFN_{NAR}-1.2). As stated above, this is probably due to hydrogen bonding with the protein matrix. This fact renders the band unsuitable for quantification purposes because of its ambiguous spectral position and because of a possible impact of hydrogen bonding on the band intensity. Finally, the bands at 1085 and 1065 cm^{-1}, which arise from aromatic skeletal vibrations of the flavone ring [53] of NAR, can also be detected in the SFN_{NAR} spectrum and are good candidates for quantification marker bands as no noticeable shift was detected between free and loaded NAR. However, the latter band is close to a maximum of SFN absorption, which makes it difficult to distinguish between NAR and SFN absorption. In contrast, the strong and sharp 1085 cm^{-1} band is located on a slope of the SFN spectrum and can, therefore, be distinguished from it and used for quantification. For this reason, we decided to use the 1085 cm^{-1} absorption band for quantification.

The next step consisted of identifying a band from the protein matrix that can be used for normalization. Here, the amide III band at 1229 cm^{-1}, which is the strongest signal from SFN in the 1350-900 cm^{-1} region, was used.

With the quantification band from the drug and the normalization band from the nanoparticle matrix identified, the spectra needed to be baseline corrected before further operations. As baseline points, we selected points at the edges of the spectra (1350 and 900 cm^{-1}), the minima on both sides of the normalization band (1316 and 1185 cm^{-1}) and one extra point close to the quantification band at a minimum of the SFN spectrum (1134 cm^{-1}). These are shown as orange dots in figure 2.

3.3. Calibration curve

The next step in the quantification process was to obtain the calibration curve between drug load and the absorbance at 1085 cm^{-1}. This was achieved by analyzing the calibration samples with known amounts of SFN and NAR. An example of a series of baseline-corrected and normalized spectra of calibration samples containing an increasing amount of NAR is presented in Figure 4a, in which the

Preprints (www.preprints.org) | NOT PEER-REVIEWED | Posted: 3 September 2020 doi:10.20944/preprints202009.0047.v1

increase in absorbance at 1085 cm^{-1} as the NAR concentration increases can be clearly seen. Fitting of the six independent calibration series, three obtained at the University of Murcia and three obtained at Stockholm University, are shown in Figure 4b. In Figure 4c, one calibration curve was fitted to all individual data points. This calibration curve was later used for quantification purposes in this work. The signal at 0 *NAR%* in Figures 4b and 4c stems from SFN absorption. The data were fitted by linear regression using the least-squares method. For the final calibration curve shown in Fig. 4c, the Y-intercept was constrained to be equal to the average value of absorbance at 0 *NAR%* of the six samples (this value remained the same even when we included the ten additional measurements of SFN blanks). We used this approach to minimize the error for determining low NAR loads, which depends strongly on the starting point of the calibration curve. The fitting parameters are collected in Table 1.

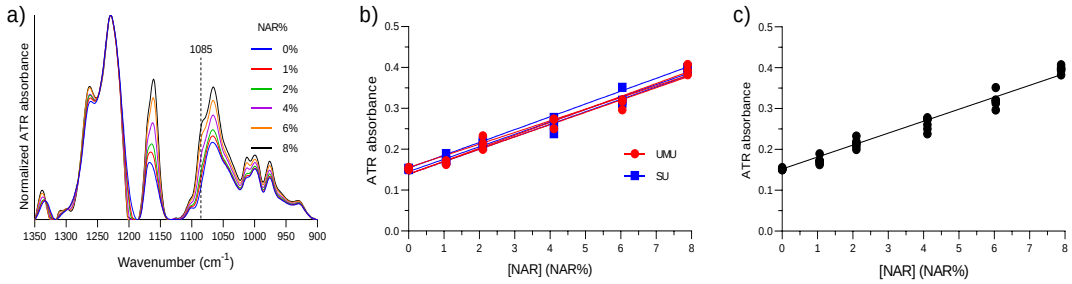

Figure 4. a) Absorbance spectra of SFN with increasing quantities of NAR; b) Six calibration data sets and their respective calibration lines, three obtained at the University of Murcia and three obtained at Stockholm University. c) Calibration data set including all data points.

Table 1. Calibration curve parameters. The first two columns list the average parameters and standard deviation (σ) for each set of three calibration lines obtained at the University of Murcia (UMU) and Stockholm University (SU). The third column lists the parameters of the calibration line fitted to all data points under the constraint of passing through the average value at 0 *NAR%*.

	UMU	SU	All data points
	Mean +/- σ		
Best-fit values			
Slope *	0.030 +/- 0.002	0.031 +/- 0.001	0.029
Y-intercept	0.145 +/- 0.009	0.146 +/- 0.008	0.152
Goodness of Fit			
R^2 **	0.978 +/- 0.007	0.982 +/- 0.019	0.973

* Slope units are $NAR\%^{-1}$

** R^2, coefficient of determination

3.4. Parameters for method validation

3.4.1. Range and linearity of the calibration curve

The linearity of the calibration data was good as indicated by the R^2 values for the individual calibration lines and for the single calibration with all data points (Table 1), which are equal to or

Preprints (www.preprints.org) | NOT PEER-REVIEWED | Posted: 3 September 2020 doi:10.20944/preprints202009.0047.v1

above 0.973. Also, a visual inspection of the residual plot (data not shown) demonstrates a linear correlation between analytical response and drug concentration over the range of 0 – 7.89 *NAR%*.

3.4.2. Robustness of the method

The robustness of the analytical method is illustrated by the strong similarities between the six calibration lines in Figure 3b measured on different days, in different laboratories and with different spectrometers. For instance, the SU Bruker spectrometer used a Mercury-Cadmium-Telluride detector and was continuously purged with CO_2-reduced, dry air, whereas, the UMU Thermo Fisher Scientific spectrometer used a Deuterated Triglycine Sulfate detector and was not purged. Despite the above, an analysis of covariance performed as described elsewhere [54] showed no significant differences between the slopes or Y-intercepts of the lines generated at the two institutions with P-values of 0.92 and 0.18, respectively. The agreement demonstrates amongst others that water vapor does not interfere with the measurements because the selected NAR band is outside the main region of water vapor absorption. The relative standard deviations calculated from the average and standard deviation of all slopes and Y-axis intercepts are 3.8% and 5.2%, respectively.

3.4.3. Limit of detection, limit of quantification and reproducibility (precision) of the method

As defined by the IUPAC Gold Book [55,56], the limit of detection (LOD) and limit of quantification (LOQ), expressed as concentration or quantity, is the smallest measured value (A), that can be detected or quantified, respectively, with reasonable certainty for a given analytical procedure. A_{LOD} and A_{LOQ} are given by equations (4) and (5), respectively [55,56]:

$$A_{LOD} = \bar{A} + 3.3\sigma, \quad (4)$$

$$A_{LOQ} = \bar{A} + 10\sigma, \quad (5)$$

where $\bar{A}$ and σ are the average and standard deviation, respectively, of the absorbance measurements at 1085 cm^{-1} for ten independent blank SFN samples, five of which were made at the University of Murcia and the other five at Stockholm University. The number of ten samples and the numerical factors of 3.3 and 10 are suggested by IUPAC according to normality and a confidence level of α = 0.05 for A_{LOD} and A_{LOQ}, respectively. The reproducibility of the method is given by the relative standard deviation of the blank measurements calculated by equation (6):

$$Reproducibility\ (\%) = \frac{\sigma}{\bar{A}} \times 100, \quad (6)$$

The ten spectra used and their absorbance at 1085 cm^{-1} are presented in Figure 5 and the evaluation is summarized in Table 2. Results for DLC_{LOD}, DLC_{LOQ} and reproducibility are also collected in Table 2. The first two were calculated by inserting A_{LOD} and A_{LOQ} into the equation for the final calibration line. This result shows the high sensitivity and precision of the analytical method developed here.

Preprints (www.preprints.org) | NOT PEER-REVIEWED | Posted: 3 September 2020 doi:10.20944/preprints202009.0047.v1

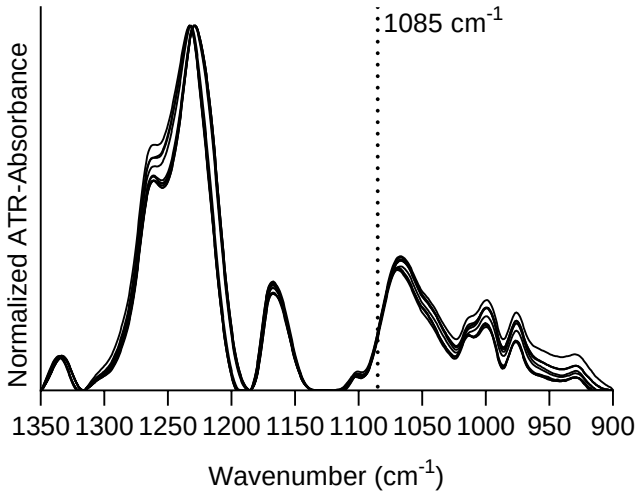

Figure 5. Baseline corrected and normalized spectra of the 10 blank SFN samples used for the calculation of limit of detection (*LOD*), limit of quantification (*LOQ*) and reproducibility for the method.

Table 2. Average ($\bar{A}$) and standard deviation (σ) of ATR-absorbance at 1085 cm^{-1} used for the calculation of limits of detection (A_{LOD} and DLC_{LOD}), limits of quantification (A_{LOQ} and DLC_{LOQ}) and reproducibility for the method according to equations 4-6.

Quantity	Value
Average of absorbance at 1085 cm^{-1} ($\bar{A}$)	0.151
Standard deviation (σ)	0.003
Reproducibility (%)	2.0
LOD of absorbance (A_{LOD})	0.161
LOQ of absorbance (A_{LOQ})	0.181
DLC_{LOD} (%)	0.3
DLC_{LOQ} (%)	1.0

3.4.4. Accuracy of the method

The accuracy of the proposed method was evaluated by the spike and recovery method [56,57]. First, a calibration sample with 4.11 *NAR*% relative mass was prepared and divided into two 200 μL aliquots. One aliquot was spiked with 5 μL of a 15 mg/mL NAR solution in EtOH to achieve a final 6.51 *NAR*% relative mass and 5 μL of EtOH were added to the other sample. The infrared spectra of spiked and unspiked samples were recorded immediately and the respective *DLC*s determined from the absorbance at 1085 cm^{-1} as described. The accuracy was expressed as the recovery % of the spiked sample as stated in equation 7. The procedure was repeated 4 times and the results are shown in Table 3. The small variation of 4% on average from the expected value denotes that the analytical procedure is accurate and that there are no matrix effects. The small error is within the expected errors of pipetting, weighing and absorbance measurement.

Preprints (www.preprints.org) | NOT PEER-REVIEWED | Posted: 3 September 2020 doi:10.20944/preprints202009.0047.v1

$$Recovery\ (\%) = \frac{DLC_{spiked} - DLC_{unspiked}}{NAR\%_{added}} \times 100, \quad (7)$$

Table 3. Evaluation of the accuracy of the method for the determination of NAR in SFN.

Sample	Recovery (%)
1	103%
2	104%
3	102%
4	106%
Average	104%
Standard deviation	2%

3.5 Drug quantification in NAR-loaded SFN

The DLC and EE of the NAR-loaded SFN samples measured with this method are presented in Table 4. An increase in the NAR concentration of the loading solution leads to a non-linear increase in DLC, most of the loading activity taking place at a low NAR concentration. This has been reported before and is attributed to saturation of the drug binding sites on the surface of the nanoparticles [15]. By contrast, the EE decreases linearly when the NAR concentration increases.

Notice that the nature of the drug can be identified by infrared spectroscopy even for the nanoparticles with the lowest drug load (Figure 1, section 3.1, Specificity of ATR-FTIR spectroscopy for identifying drugs in SFN), although their determined *DLC* is close to the detection limit as it lies between the DLC_{LOQ} and DLC_{LOD}.

Table 4. Drug loading content (DLC) and entrapment efficiency (EE) of NAR-loaded SFN are expressed as mean +/- standard deviation. n = 3

Sample	*DLC* (%)	*EE* (%)
	Mean +/- σ (RSD)	
SFN_{NAR}-0.3	0.87 +/- 0.07 (8.7%)	41.0 +/- 3.0 (7.3%)
SFN_{NAR}-1.2	3.13 +/- 0.08 (2.6%)	38.0 +/- 1.0 (2.6%)
SFN_{NAR}-4.5	4.06 +/- 0.06 (1.6%)	13.2 +/- 0.2 (1.5%)

*RSD, relative standard deviation

The relative standard deviation of the measured *DLC* values are noteworthy low for measurement above the DLC_{LOQ} of 1.0% (table 4), especially when compared to UV-visible spectroscopy and high-performance liquid chromatography measurements used by the direct or indirect methods mentioned in Introduction. Based on our experience, the coefficient of variations for these methods tend to be much larger, ranging from several percent to over 10%, mostly due to large dilution of the supernatants needed (up to 1:500) and the unreliable phase separation through centrifugation (data not shown). These large and sometimes unacceptable deviations were the primary reasons to motivate this work in the first place. The problems involved will be discussed in the following at the example of the SFN_{NAR}-4.5 mg/mL sample. To calculate its *DLC* by the indirect approach, particles need to be separated from the initially 4.5 mg/mL NAR solution after the loading phase. Assuming a complete removal and an EE is 15% (close to what was obtained here, see table 4), the drug concentration in the supernatant will be close to 3.8 mg/ml corresponding to 85% of the

 doi:10.20944/preprints202009.0047.v1

total drug feed. Such a high concentration cannot be directly detected with conventional UV-visible spectrometers. In the case of NAR dissolved in EtOH, an absorbance of 1.0 is achieved with a concentration of 0.015 mg/mL at 289 nm (10 mm path length cuvette). This means that in order to bring the concentration of a 3.8 mg/mL sample to the concentration range suitable for UV-Visible spectroscopy, a 1:250 dilution is needed which carries a high degree of error. Assuming a two-step dilution – corresponding to four pipetted volumes – and assuming a pipetting error of 2%, the final concentration error is close to 4%. The situation improves at lower concentrations of the loading solution were the EE is higher. For example, the SFN$_{NAR}$-0.3 sample with an EE close to 50% would require only a 1:10 dilution. However, only low *DLC*s are achieved with such low drug concentrations, whereas high *DLC*s are the aim of drug producers. Thus, the dilution error of the indirect approach is highest under the conditions that are most interesting from a drug manufacturing point of view, whereas they are lowest for the direct method presented in this work. Furthermore, the separation of SFN from the NAR loading solution is ineffective. Control samples containing 1 mg/mL of SFN dispersed in 30% EtOH, had an absorbance greater than 0.100 at 289 nm after attempted separation of SFN from the solution phase by centrifugation for 30 minutes at 13.400 rpm. The absorbance stems from the nanoparticles and adds up to the absorbance of the drug in a quantification experiment, making the apparent absorbance of the drug larger than it actually is. This generates a systematic error, which is particularly pronounced at low *NAR%*. This error exists in all cases where the measured spectroscopic signal of the drug overlaps with absorption of the nanoparticle carrier. Then, the indirect approach is prone to errors in the entire concentration range of the drug, either due to incomplete separation of drug from nanoparticles at low drug concentrations or due to dilution errors at high drug concentrations.

section may be divided by subheadings. It should provide a concise and precise description of the experimental results, their interpretation as well as the experimental conclusions that can be drawn.

4. Conclusions

A straightforward, economic and fast method for drug quantification in nanoparticles was developed using ATR-FTIR spectroscopy of dry films. The method presents excellent linearity in the range of 0.00 to 7.89 *NAR%* despite the low drug concentrations. The *DLC*$_{LOD}$ and *DLC*$_{LOQ}$ were 0.3 and 1.0%, respectively, for NAR in SFN. Reproducibility in terms of relative standard deviation after measuring 10 blank samples was 2.0%. The method was seen to be robust as calibration lines measured in two different institutions showed no statistical differences.

The methodology developed here is less susceptible to the over- or underestimation of *DLC* using conventional direct and indirect approaches [30,31] and can be easily extrapolated to other drug-loaded SFN and even to other polymeric nanocarriers. Furthermore, it can operate on the final drug product without the need to have access to the loading solution. Here, it is faster than the direct approach because it does not require drug extraction and phase separation.

In the present case, a simple evaluation of the absorbance at one particular wavenumber was sufficient for quantifying a drug in protein nanoparticles. Other drugs and carrier systems might present more challenging cases and require tailored approaches for the evaluation. These could consist of considering (i) the signal at several wavenumbers to eliminate the protein contribution to the measured signal, (ii) the second derivative of absorbance for a better separation of drug and protein bands, and (iii) the use of multivariate statistical methods to identify relevant spectral regions and to establish calibration models. However, in all cases, it would be beneficial to base the quantification on drug bands which are little affected by the environment, i.e. bands which are caused by vibrations with small contributions from functional groups able to interact with the protein matrix. For this reason, we used the band of a skeletal aromatic vibration at 1085 cm^{-1} and discarded the use of the stronger OH band at 1156 cm^{-1}, which shifted when the drug was incorporated into the protein matrix.

Author Contributions: Conceptualization, G.C. and A.B.; methodology and preparation of SF nanoparticles, G.C. and M.G.M.; investigation, G.C. and A.B.; writing—original draft preparation, G.C. and A.B.; writing—review & editing, G.C., GV and A.B.; supervision, A.B. and G.V.; funding acquisition, A.B. and G.V. All authors have read and agreed to the published version of the manuscript.

Funding: This work has been partially supported from the European Commission (FEDER/ERDF) and the Spanish MINECO (Ref. CTQ2017-87708-R) and the programme of support to the research of the Seneca Foundation of Science and Technology of Murcia, Spain (Ref. 20977/PI/18). G. Carissimi acknowledges support from the University of Murcia through the Mare Nostrum lines of action scholarship for 2018-2019 (R-421-2019). The infrared spectrometer was funded by the Knut and Alice Wallenberg foundation.

Acknowledgments: The authors wish to thank the Department of Biotechnology of the Instituto Murciano de Investigación y Desarrollo Agrario y Alimentario (IMIDA) for providing the silk cocoons used in this study.

Conflicts of Interest: The authors declare no conflict of interest. The funders had no role in the design of the study; in the collection, analyses, or interpretation of data; in the writing of the manuscript, or in the decision to publish the results.

References

1 Bobo D, Robinson KJ, Islam J, *et al.* Nanoparticle-Based Medicines: A Review of FDA-Approved Materials and Clinical Trials to Date. *Pharm Res* 2016; **33**: 2373-2387

2 Kalepu S, Nekkanti V. Insoluble drug delivery strategies: Review of recent advances and business prospects. *Acta Pharm Sin B* 2015; **5**: 442-453

3 Karimi M, Ghasemi A, Sahandi Zangabad P, *et al.* Smart Micro/Nanoparticles in Stimulus-Responsive Drug/Gene Delivery Systems. Vol 45. Royal Society of Chemistry; 2016.

4 Montalbán MG, Carissimi G, Lozano-Pérez AA, *et al.* Biopolymeric Nanoparticle Synthesis in Ionic Liquids. *Recent Adv Ion Liq* 2018; **i**: 3-26

5 Matsumura Y, Maeda H. A New Concept for Macromolecular Therapeutics in Cancer Chemotherapy: Mechanism of Tumoritropic Accumulation of Proteins and the Antitumor Agent Smancs. *Cancer Res* 1986; **46**: 6387-6392

6 Fang J, Islam R, Islam W, *et al.* Augmentation of EPR Effect and Efficacy of Anticancer Nanomedicine by Carbon Monoxide Generating Agents. *Pharmaceutics* 2019; **11**: 343

7 Elzoghby AO, Samy WM, Elgindy NA. Albumin-based nanoparticles as potential controlled release drug delivery systems. *J Control Release* 2012; **157**: 168-182

8 Barenholz Y. Doxil® - The first FDA-approved nano-drug: Lessons learned. *J Control Release* 2012; **160**: 117-134

9 Lim SB, Banerjee A, Önyüksel H. Improvement of drug safety by the use of lipid-based nanocarriers. *J Control Release* 2012; **163**: 34-45

10 Ding B, Wahid MA, Wang Z, *et al.* Triptolide and celastrol loaded silk fibroin nanoparticles show synergistic effect against human pancreatic cancer cells. *Nanoscale* 2017; **9**: 11739-11753

11 Zhao Z, Li Y, Xie M Bin. Silk fibroin-based nanoparticles for drug delivery. *Int J Mol Sci* 2015; **16**: 4880-4903

12 Mottaghitalab F, Farokhi M, Shokrgozar MA, *et al.* Silk fibroin nanoparticle as a novel drug delivery system. *J Control Release* 2015; **206**: 161-176

13 Montalbán M, Coburn J, Lozano-Pérez A, *et al.* Production of Curcumin-Loaded Silk Fibroin Nanoparticles for Cancer Therapy. *Nanomaterials* 2018; **8**: 126

14 Raveendran P, Fu J, Wallen SL. Completely 'Green' Synthesis and Stabilization of Metal Nanoparticles. *J Am Chem Soc* 2003; **125**: 13940-13941

15 Lozano-Pérez AA, Rivero HC, Pérez Hernández M del C, *et al.* Silk fibroin nanoparticles: Efficient vehicles for the natural antioxidant quercetin. *Int J Pharm* 2017; **518**: 11-19

16 Fuster MG, Carissimi G, Montalbán MG, *et al.* Improving Anticancer Therapy with Naringenin-Loaded Silk Fibroin Nanoparticles. *Nanomaterials* 2020

17 Mathur AB, Gupta V. Silk fibroin-derived nanoparticles for biomedical applications. 2010; **5**: 807-820

18 Tian Y, Jiang X, Chen X, *et al.* Doxorubicin-loaded magnetic silk fibroin nanoparticles for targeted therapy of multidrug-resistant cancer. *Adv Mater* 2014; **26**: 7393-7398

19 Amgoth C, Dharmapuri G. Synthesis and Characterization of Polymeric Nanoparticles and Capsules as Payload for Anticancer Drugs and Nanomedicines. *Mater Today Proc* 2016; **3**: 3833-3837

20 Bian X, Wu P, Sha H, *et al.* Anti-EGFR-iRGD recombinant protein conjugated silk fibroin nanoparticles for enhanced tumor targeting and antitumor efficiency. *Onco Targets Ther* 2016; **9**: 3153-3162

21 Kumari A, Yadav SK, Pakade YB, *et al.* Development of biodegradable nanoparticles for delivery of quercetin. *Colloids Surfaces B Biointerfaces* 2010; **80**: 184-192

22 Trucillo P, Campardelli R, Reverchon E. Supercritical CO2 assisted liposomes formation: Optimization of the lipidic layer for an efficient hydrophilic drug loading. *J CO2 Util* 2017; **18**: 181-188

23 Seib FP, Jones GT, Rnjak-Kovacina J, *et al.* pH-Dependent anticancer drug release from silk nanoparticles. *Adv Healthc Mater* 2014; **2**: 1-13

24 Subia B, Kundu SC. Drug loading and release on tumor cells using silk fibroin-albumin nanoparticles as carriers. *Nanotechnology* 2013; **24**

25 Wongpinyochit T, Uhlmann P, Urquhart AJ, *et al.* PEGylated Silk Nanoparticles for Anticancer Drug Delivery. *Biomacromolecules* 2015; **16**: 3712-3722

26 Suktham K, Koobkokkruad T, Wutikhun T, *et al.* Efficiency of resveratrol-loaded sericin nanoparticles: Promising bionanocarriers for drug delivery. *Int J Pharm* 2018; **537**: 48-56

27 Pham DT, Saelim N, Tiyaboonchai W. Paclitaxel loaded EDC-crosslinked fibroin nanoparticles: a potential approach for colon cancer treatment. *Drug Deliv Transl Res* 2020; **10**: 413-424

28 Wu J, Wang J, Zhang J, *et al.* Oral Delivery of Curcumin Using Silk Nano- and Microparticles. *ACS Biomater Sci Eng* 2018; **4**: 3885-3894

29 Perteghella S, Sottani C, Cocc V, *et al.* Paclitaxel-Loaded Silk Fibroin Nanoparticles : Method Validation by UHPLC-MS / MS to Assess an Exogenous Approach to Load Cytotoxic Drugs.

30 Wallace SJ, Li J, Nation RL, *et al.* Drug release from nanomedicines: selection of appropriate encapsulation and release methodology. *Drug Deliv Transl Res* 2012; **2**: 284-292

31 Lv Y, He H, Qi J, *et al.* Visual validation of the measurement of entrapment efficiency of drug nanocarriers. *Int J Pharm* 2018; **547**: 395-403

32 Khanmohammadi M, Mobedi E, Garmarudi AB, *et al.* Simultaneous determination of levodopa and carbidopa in levodopa-carbidopa tablets by ATR-FTIR spectrometry. *Pharm Dev Technol* 2007; **12**: 573-580

33 Koleva BB, Kolev TM, Tsalev DL, *et al.* Determination of phenacetin and salophen analgetics in solid binary mixtures with caffeine by infrared linear dichroic and Raman spectroscopy. *J Pharm Biomed Anal* 2008; **46**: 267-273

34 de la Asunción-Nadal V, Armenta S, Garrigues S, *et al.* Identification and determination of synthetic cannabinoids in herbal products by dry film attenuated total reflectance-infrared spectroscopy. *Talanta* 2017; **167**: 344-351

35 Wartewig S, Neubert RHH. Pharmaceutical applications of Mid-IR and Raman spectroscopy. *Adv Drug*

Deliv Rev 2005; **57**: 1144-1170

36 Kalinkova GN. Infrared spectroscopy in pharmacy. *Vib Spectrosc* 1999; **19**: 307-320

37 Bunaciu AA, Aboul-Enein HY, Fleschin S. Application of fourier transform infrared spectrophotometry in pharmaceutical drugs analysis. *Appl Spectrosc Rev* 2010; **45**: 206-219

38 Pandey RP, Gurung RB, Sohng JK. Dietary sources, bioavailability and biological activities of naringenin and its derivatives. *Nov Sci* 2015

39 Kawaii S, Tomono Y, Katase E, *et al.* Quantitation of flavonoids constituents in Citrus fruits. *J Agric Food Chem* 1999; **47**: 3565-3571

40 Treml J, Šmejkal K. Flavonoids as Potent Scavengers of Hydroxyl Radicals. *Compr Rev Food Sci Food Saf* 2016; **15**: 720-738

41 Bodet C, La VD, Epifano F, *et al.* Naringenin has anti-inflammatory properties in macrophage and ex vivo human whole-blood models. *J Periodontal Res* 2008; **43**: 400-407

42 Liao ACH, Kuo CC, Huang YC, *et al.* Naringenin inhibits migration of bladder cancer cells through downregulation of AKT and MMP-2. *Mol Med Rep* 2014; **10**: 1531-1536

43 Bao L, Liu F, Guo H bin, *et al.* Naringenin inhibits proliferation, migration, and invasion as well as induces apoptosis of gastric cancer SGC7901 cell line by downregulation of AKT pathway. *Tumor Biol* 2016; **37**: 11365-11374

44 Gumushan Aktas H, Akgun T. Naringenin inhibits prostate cancer metastasis by blocking voltage-gated sodium channels. *Biomed Pharmacother* 2018; **106**: 770-775

45 Rajamani S, Radhakrishnan A, Sengodan T, *et al.* Augmented Anticancer Activity of Naringenin-loaded TPGS Polymeric Nanosuspension for Drug Resistive MCF-7 Human Breast Cancer Cells. *Drug Dev Ind Pharm* 2018; **0**: 1-32

46 Lim W, Park S, Bazer FW, *et al.* Naringenin-Induced Apoptotic Cell Death in Prostate Cancer Cells Is Mediated via the PI3K/AKT and MAPK Signaling Pathways. *J Cell Biochem* 2017; **118**: 1118-1131

47 Boulet-Audet M, Buffeteau T, Boudreault S, *et al.* Quantitative determination of band distortions in diamond attenuated total reflectance infrared spectra. *J Phys Chem B* 2010; **114**: 8255-8261

48 Goormaghtigh E, Raussens V, Ruysschaert JM. Attenuated total reflection infrared spectroscopy of proteins and lipids in biological membranes. *Biochim Biophys Acta - Rev Biomembr* 1999; **1422**: 105-185

49 Hu X, Kaplan D, Cebe P. Determining beta-sheet crystallinity in fibrous proteins by thermal analysis and infrared spectroscopy. *Macromolecules* 2006; **39**: 6161-6170

50 Kumar S, Singh SK. Fabrication and characterization of fibroin solution and nanoparticle from silk fibers of Bombyx mori. *Part Sci Technol* 2017; **35**: 304-313

51 Carissimi G, Lozano-pérez AA, Montalbán MG, *et al.* Revealing the influence of the degumming process in the properties of silk fibroin nanoparticles. *Polymers (Basel)* 2019; **11**: 1-21

52 Baranović G, Šegota S. Infrared spectroscopy of flavones and flavonols. Reexamination of the hydroxyl and carbonyl vibrations in relation to the interactions of flavonoids with membrane lipids. *Spectrochim Acta - Part A Mol Biomol Spectrosc* 2018; **192**: 473-486

53 Machado NFL, Carvalho LAEB De, Otero JC, *et al.* A conformational study of hydroxyflavones by vibrational spectroscopy coupled to DFT calculations. *Spectrochim Acta Part A Mol Biomol Spectrosc* 2013; **109**: 116-124

54 Zar JH. Biostatistical analysis, 2nd ed. In Prentice-Hall, 1984.

55 Nič M, Jirát J, Košata B, *et al.*, eds. IUPAC Compendium of Chemical Terminology. Research Triagle Park, NC: IUPAC; 2009.

 doi:10.20944/preprints202009.0047.v1

56 Thompson M, Ellison SLR, Wood R. Harmonized guidelines for single-laboratory validation of methods of analysis (IUPAC Technical Report). *Pure Appl Chem* 2002; **74**: 835-855

57 Pandey S, Pandey P, Tiwari G, *et al.* FTIR spectroscopy: A tool for quantitative analysis of ciprofloxacin in tablets. *Indian J Pharm Sci* 2012; **74**: 86-90